Indonesian Physical Review
Volume 08 Issue 01, January 2025
P-ISSN: 2615-1278, E-ISSN: 2614-7904

Modeling of Three-Dimensional Subsurface Structures Based on Gravity Anomaly in Southwest Sumba Indonesia

Adinda Novitri[1,3], Relly Margiono[1,2,3*], Anggi Pevriadi[1,3], Hilmi Zakariya[1,3], Yan Adi Segoro[1,3]
[1] *Prodi Geofisika, Sekolah Tinggi Meteorologi Klimatologi dan Geofisika, Kota Tangerang, Indonesia*
[2] *School of Physic, Chemistry and Earth Sciences, University of Adelaide, Adelaide, Australia*
[3] *Meteorological, Climatological and Geophysical Agency, Indonesia.*

Corresponding Authors E-mail: relly.margiono@stmkg.ac.id

Article Info

Article info:
Received: 29-08-2024
Revised: 26-12-2024
Accepted: 10-01-2025

Keywords:
Faults; Gravity Anomaly; Modeling

How To Cite:
A. Novitri, R. Margiono, A. Pevriadi, H. Zakariya and Y.A. Segoro, "Modeling of Three-Dimensional Subsurface Structures Based on Gravity Anomaly in Southwest Sumba Indonesia", Indonesian Physical Review, vol. 8, no. 1, p 253-267, 2025.

DOI:
https://doi.org/10.29303/ipr.v8i1.346

Abstract

Modeling subsurface conditions using gravity anomaly data, focusing on density contrasts, provides critical insights into subsurface structures and supports identifying rock types. This study aims to define residual gravity anomalies in the Sumba region and utilize them to develop a three-dimensional subsurface model of Southwest Sumba, characterizing density contrasts and associated rock formations. Gravity data from the TOPEX dataset were employed in this research. The Airy isostasy model was applied to separate regional and residual anomalies, followed by a three-dimensional inversion using the Generalized Cross-Validation (GCV) method. The results reveal residual gravity anomalies range from -170 mGal to 211 mGal, with the Java Trench exhibiting the highest anomaly. The 3D modeling shows a relatively homogeneous density contrast at shallow depths, transitioning to more erratic variations at greater depths, extending to 15 km beneath Southwest Sumba Island. Furthermore, the calculated densities are consistent with the region's known geological background. The Java Trench, located south of Sumba, notably demonstrates a consistently high-density contrast from shallow to deeper depths, highlighting its tectonic complexity.

Introduction

The island of Sumba has a distinctive position about the Sunda-Banda arc, representing an isolated piece of continental crust against the volcanically active island arc (Sumbawa, Flores) within the forearc basin (Figure 1). The island is situated within the transition zone of the Sunda-Banda Arc, where the tectonic setting shifts from subduction processes along the Sunda Arc to an arc-continent collision along the Banda Arc [1]. The subduction and collision in this region are caused by the northward movement of the oceanic lithosphere of the Indo-Australian plate and the Australian continental lithosphere [2], [3]. The difference in the convergence speed of the oceanic plate (60-70 mm/year) [4] and the continental plate (70 mm/year) [5] certainly has implications for the geological and geodynamic order in this transition zone. One of the manifestations of the dynamics of the earth is seismic activity [6].

The east of Sumba Island tends to have little seismic activity, possibly due to the arc-continent collision. Meanwhile, the west of Sumba Island tends to have high seismic activity and is dominated by normal fault earthquakes around the trough. This pattern indicates the heterogeneity of the subsurface structure of the transition zone [7].

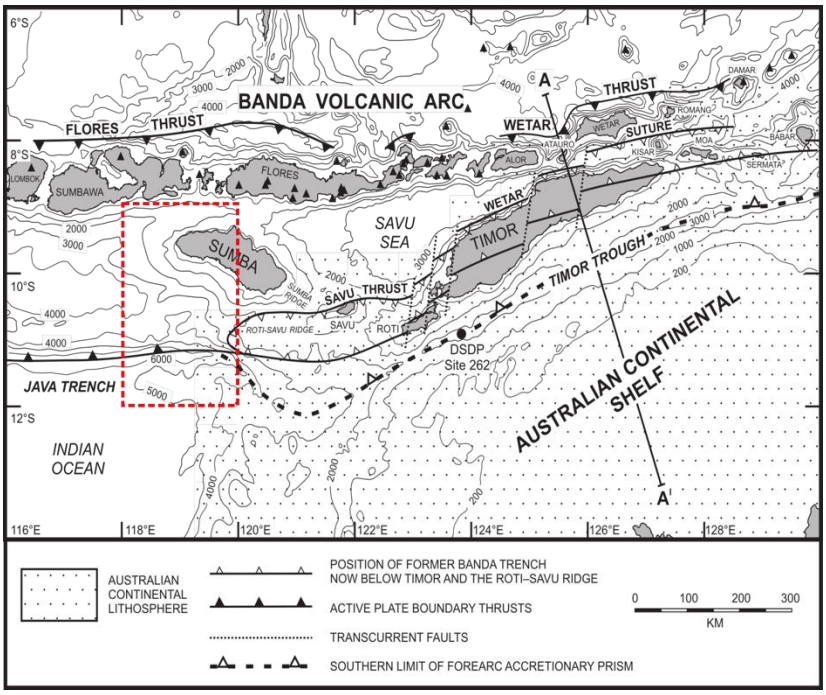

Figure 1. Geological setting of surrounding Sumba Island with a figure from [1]. A red dashed line depicts the Research area in South-West Sumba, Indonesia (9o – 12o S and 118o – 120o E).

The presence of a fault can offer both benefits and risks. While it may be a source of economically valuable minerals, it can also cause tectonic earthquakes due to fault movements. Therefore, identifying active fault structures and maintaining a fault database is crucial for disaster mitigation [8], [9]. By mapping these faults, communities can be better prepared for potential earthquakes. However, this mapping can be challenging, especially when faults are hidden beneath the surface. To overcome this, seismic and non-seismic (geopotential) methods provide valuable tools for fault identification.

Geopotential methods such as magnetic and gravity are geophysical methods that can depict subsurface structures [10]. The use of gravity data has gained popularity recently due to the availability of satellite-based datasets such as TOPEX [11], GOCE, and GRACE [12] and some gravity models[13], [14]. These satellite gravity data can assist in identifying fault structures through derivative methods, including the First Horizontal Derivative (FHD) and Second Vertical Derivative (SVD) [15], [16], [17] or to identify the sediment thickness [18] [19].

Gravity methods have been effectively utilized for fault identification in the Southwest Sumba region, as evidenced by previous research [15]. Building upon these findings, this study aims to refine subsurface interpretation by integrating residual gravity anomalies as input for three-dimensional modeling. The modeling process focuses on characterizing the density contrast within the Southwest Sumba region, enabling a more detailed understanding of subsurface structures. By linking the residual anomalies to the 3D model, this approach provides insights

into density variations, which are critical for interpreting the geological and tectonic framework of the region.

Experimental Method

The data utilized in this research were derived from satellite gravity models, specifically from CryoSat-2, Envisat, Jason-1, Geosat, and ERS-1, collectively referred to as Topex data [20], [21], [22]. This satellite data is particularly suitable for the study area (Figure 1, marked by the red dashed line), which is primarily located in the ocean, as Topex data is believed to provide more accurate gravity data in oceanic areas compared to continental regions. The satellite data were retrieved via the following link: https://topex.ucsd.edu/cgi-bin/get_data.cgi.

The datasets obtained include Free Air Anomaly (FAA) and topographic data, both provided in a gridded format (point data). The gravity data corresponds to version V32.1, while the topography data corresponds to version V27.1. Figure 2 visualizes the data after converting it from point data to raster format. The topography data displays a wide range of elevations, from the depths of the Java Trench (approximately -7000 m, depicted in dark blue) to the elevated regions of Sumba Island (~800 m). The FAA distribution shows the highest anomalies over the inland areas, with lower FAA values primarily found in the ocean.

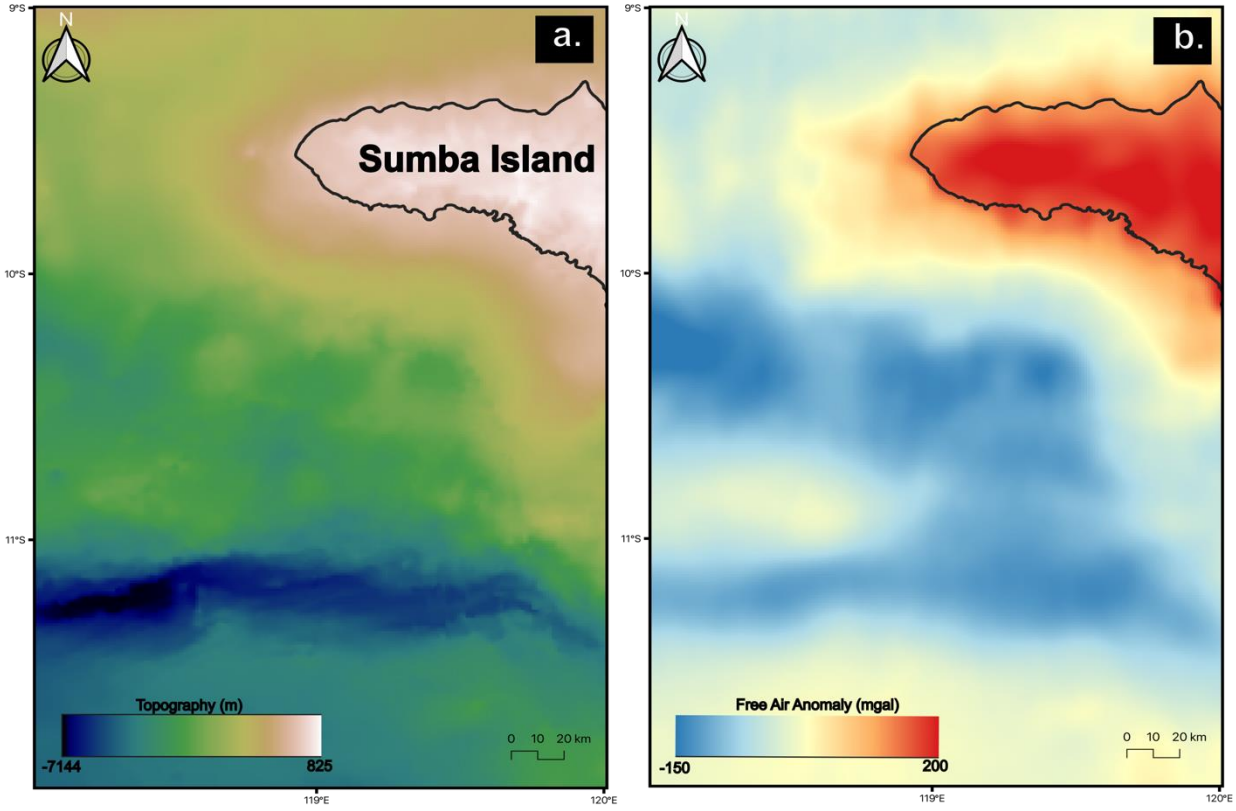

Figure 2. Topography and Free Air Anomaly maps from the data source in the WGS 84 coordinate. The point data are rasterized using TIN interpolation with a resolution of 0.01 x 0.01 pixel and using the cubic method.

The first step of processing is to determine the average density (ρ) of the research area using the Parasnis method [23], the slope value between FAA and topographic data. However, we find the density value is too small, which is 0.6 g/cm^3, and does not match typical rock densities. Because of that, we prefer to use a commonly used average crustal density for Bouguer correction, which is 2.67 g/cm^3 for the area equal to or more than 0 Mean Seal Level (MSL), and we use differences between crustal density and water density for the area in the ocean (2.67 g/cm^3 – 1.04 g/m^3). The density value is then used to compute the Bouguer correction Bc Using Eq. (1). The second step is to calculate the Simple Bouguer Anomaly (SBA) Value using Eq. (2). After obtaining the SBA value, the calculation continues to produce Complete Bouguer Anomaly (CBA) by adding SBA with Terrain Correction (Tc). Terrain correction is achieved through forward modeling, which requires constructing a 3D model of basic geometric shapes. In this study, we utilized rectangular prisms to represent the topographic masses. The gravitational influence of each prism is then calculated at each designated computation point. We used the terrain correction algorithm [24] provided in the Harmonica package [25]. To accomplish this, a regular grid of topographic heights, or Digital Elevation Model (DEM), for the Sumba region is required. We utilized the same topographic data from the Topex website, extending the grid with an additional 1-degree buffer beyond the original research area in Figure 3.

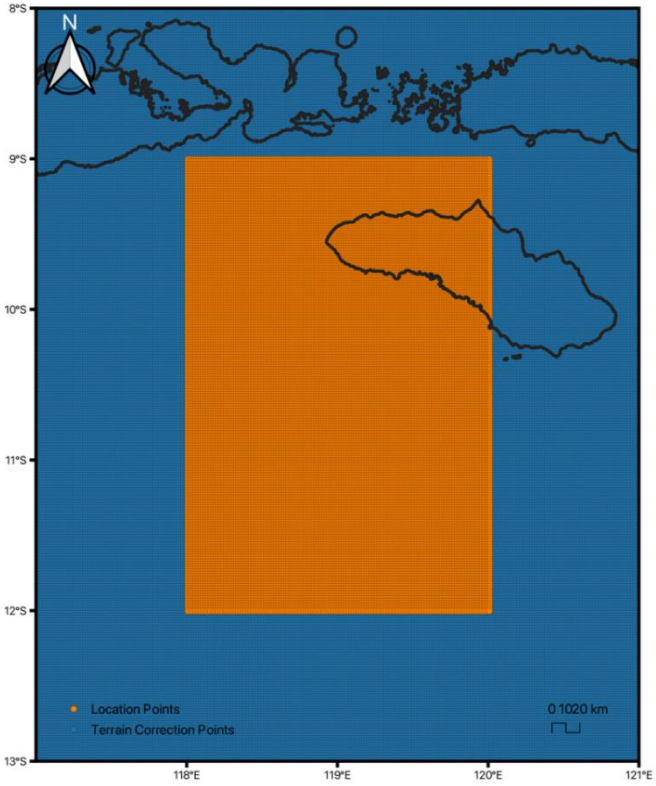

Figure 3. The region used for terrain correction consists of internal and external bounds. The internal bound, represented by orange dots, marks the primary locations for gravity data collection, while the external bound is shown with blue dots. Both bounds utilize topography data from V27.1 obtained from the TOPEX website.

$$Bc = 0.04193\rho h \quad (1)$$

$$SBA = FAA - Bc \quad (2)$$

$$CBA = SBA + Tc \quad (3)$$

Following the calculation of the CBA, the next step is to separate the regional and residual anomalies. The CBA is largely affected by variations in Moho depth due to significant density contrasts and thicknesses. To isolate the signal from the shallower intrusions within the study area, referred to as the residual, removing the influence of deeper, more extensive sources, known as the regional component, is essential. In this study, we generate the residual anomaly by modeling and removing the Moho effect using an Airy isostasy model, assuming all topography is locally compensated by variations in Moho depth [24]. The residual anomaly calculations were performed using the Harmonica package [25].

The final step involves modeling the 3D subsurface structure of the gravity anomaly data. For this purpose, the Grav3D package was utilized to analyze variations in subsurface density across the study area. A three-dimensional mesh was constructed with dimensions of 125 × 125 × 150, representing the easting, northing, and vertical directions, respectively. The cell sizes in each direction correspond to distances of 1760 meters, 2656 meters, and 100 meters, respectively. This configuration results in a horizontal area of 220 km × 332 km, covering 72,040 km², with a vertical extent of 15 km.

Residual gravity data served as the primary input for the inversion process, and Gaussian noise was added to the dataset prior to inversion to simulate realistic conditions. A noise level of 0.01% was specified for both the percentage and minimum values, ensuring a virtually noise-free dataset. The inversion was performed using default parameters, including depth weighting, wavelet compression, initial model configuration, length scales, bounds, and reference model settings. The Generalized Cross-Validation (GCV) [26] method was employed as the inversion mode. Additionally, the topography used in the model was sourced from the TOPEX dataset, maintaining consistency across the analysis.

Results and Discussion

The Simple Bouguer Anomaly (SBA) and Complete Bouguer Anomaly (CBA) results are depicted in Figures 4a and 4b, respectively. The spatial distribution of anomalies indicates that high anomaly values are concentrated in the Java Trench and its surrounding regions, whereas low anomaly values are primarily associated with Sumba Island. The SBA values range from 51 mGal to 394 mGal, while the CBA values range from 85 mGal to 860 mGal. This difference underscores the importance of considering terrain corrections when calculating gravity anomalies, as terrain variations significantly influence the results.

The variation between SBA and CBA results emphasizes the critical role of accurate terrain modelling in geophysical analyses. The inclusion of terrain corrections in the calculation of the CBA accounts for the gravitational effects of topographic masses, leading to higher anomaly values compared to the SBA. This adjustment provides a more precise representation of the subsurface density variations and geological features. The Java Trench, associated with subduction processes, shows high anomalies due to dense materials in the crust, while Sumba

Island's lower anomalies suggest less dense or structurally distinct materials. These findings provide valuable insights into regional tectonic and geological processes.

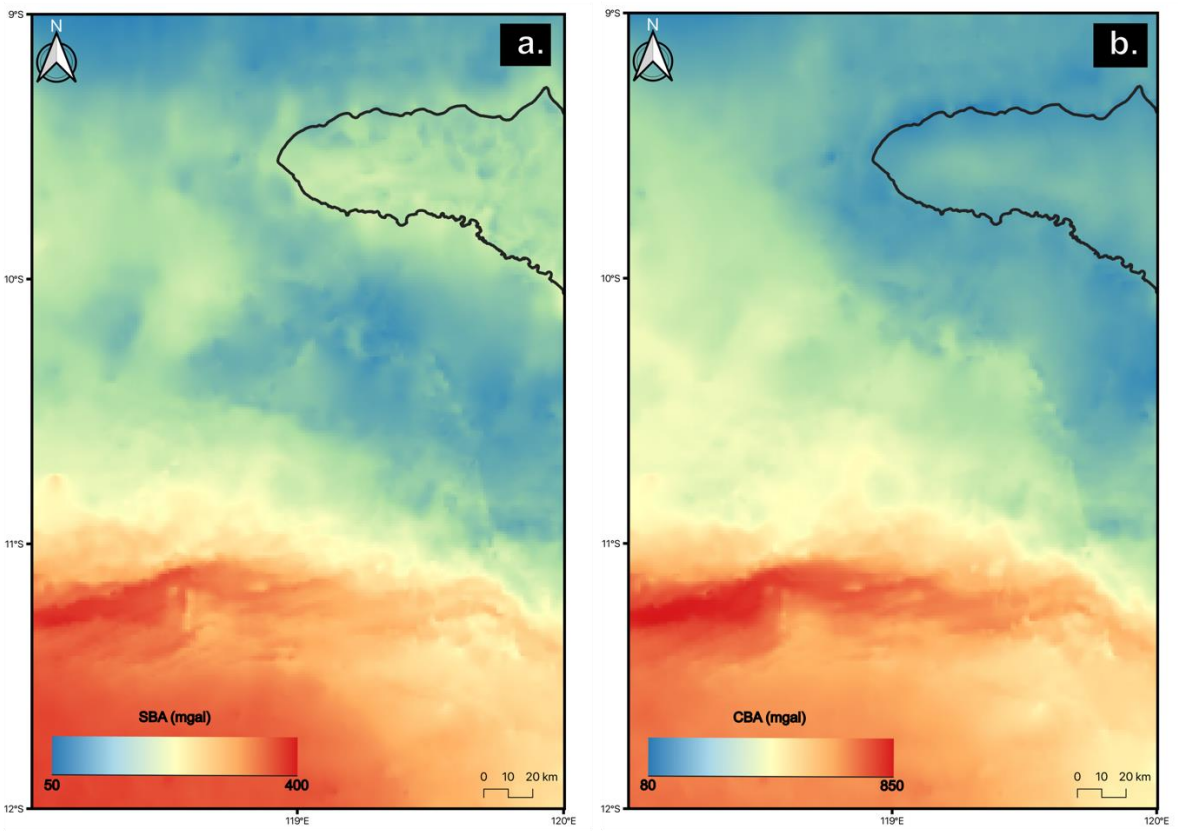

Figure 4. Simple Bouguer Anomaly (a) and Complete Bouguer Anomaly (b) in the WGS 84 coordinate. The point data are rasterized using TIN interpolation with resolution 0.01 x 0.01 pixel and cubic method.

The Complete Bouguer Anomaly (CBA) presented in the previous figure reflects the combined contributions of both shallow and deep sources. A separation of regional and residual anomalies is required to better distinguish these sources. The regional anomaly represents contributions from deeper geological structures, while the residual anomaly corresponds to the influence of shallower sources. This separation clarifies the subsurface features at different depths, allowing for more detailed interpretations of the gravitational field.

The results of the anomaly separation are shown in Figures 5a and 5b. The regional anomaly (Figure 5a) highlights the broader, deeper features of the study area, with values ranging from 110 mGal to 757 mGal. In contrast, the residual anomaly (Figure 5b) emphasizes localized, shallow features, ranging from -170 mGal to 211 mGal. This differentiation reveals the dominance of deep-seated structures in shaping the regional gravitational field while allowing the residual anomaly to isolate and highlight near-surface variations. Such a separation is critical for interpreting geological processes and structures at varying depths.

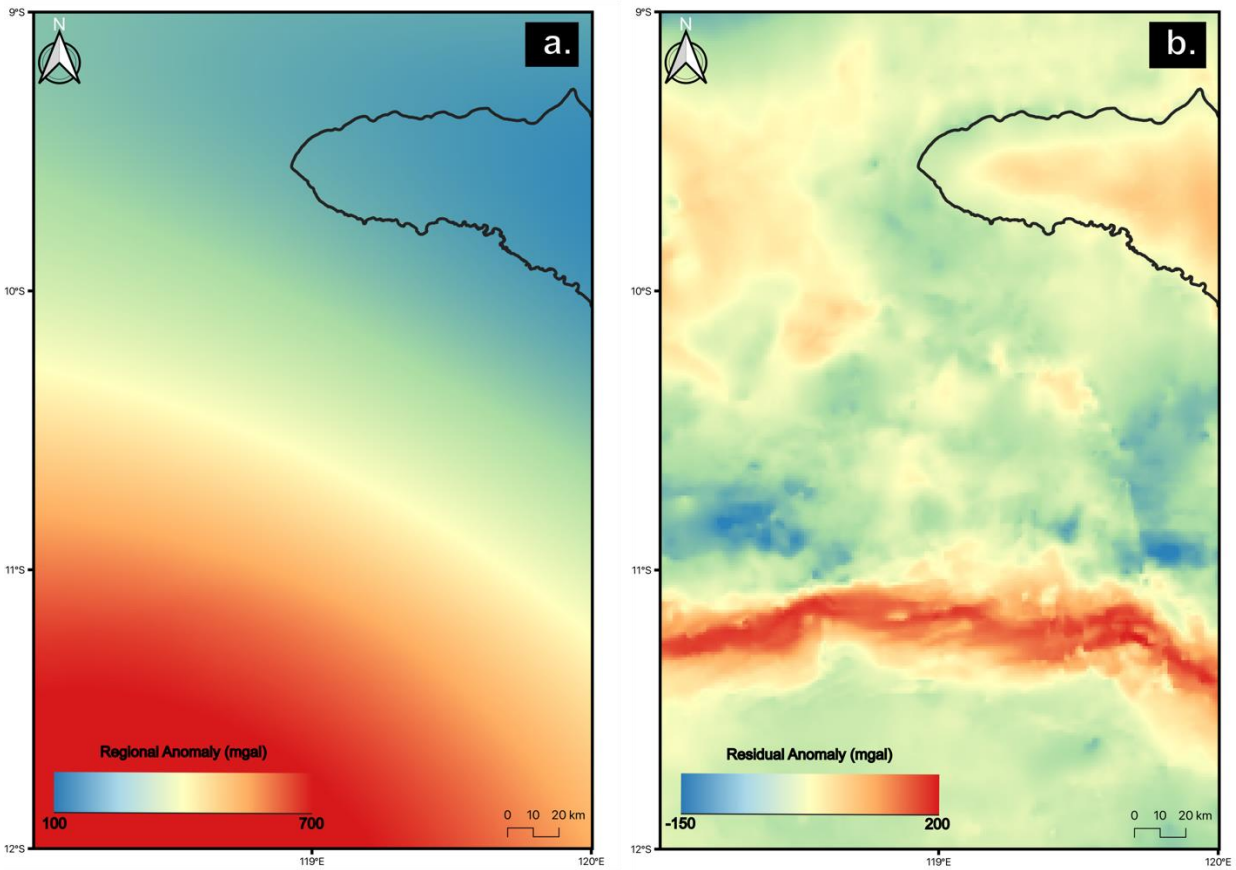

Figure 5. Map of regional anomalies (a) and residual anomalies (b). The regional and residual separation are calculated using the harmonica [25] package using the airy isostasy model. The point data are rasterized using TIN interpolation with a resolution of 0.01 x 0.01 pixel and using the cubic method.

Based on the residual anomaly (Figure 5b), residual profiles were extracted along two selected transects, A-A′ and B-B′, as shown in Figure 6. These profiles provide insights into the subsurface structures along their respective lines. The residual anomaly profile along line A-A′ begins in the northern part of the study area and shows a notable increase in residual values as it crosses Sumba Island, reaching approximately 100 mGal. Southward, as the profile traverses the ocean region, the residual values exhibit fluctuations characterized by alternating increases and decreases. Interestingly, a sharp change is observed as the profile intersects the Java Trench or subduction zone, where residual values peak at approximately 200 mGal. This sharp gradient likely reflects the tectonic complexity and density variations associated with the subduction process.

For the residual anomaly profile along line B-B′, which starts west from an oceanic region, the profile initially displays a general decline in residual values, reaching a minimum of approximately -40 mGal. As the profile approaches Sumba Island, residual values rise, suggesting the influence of near-surface density variations associated with the island's geological structures. This trend indicates the contrasting density properties of oceanic and

terrestrial regions and highlights the importance of profile-based analysis for understanding subsurface density distribution in tectonically active regions.

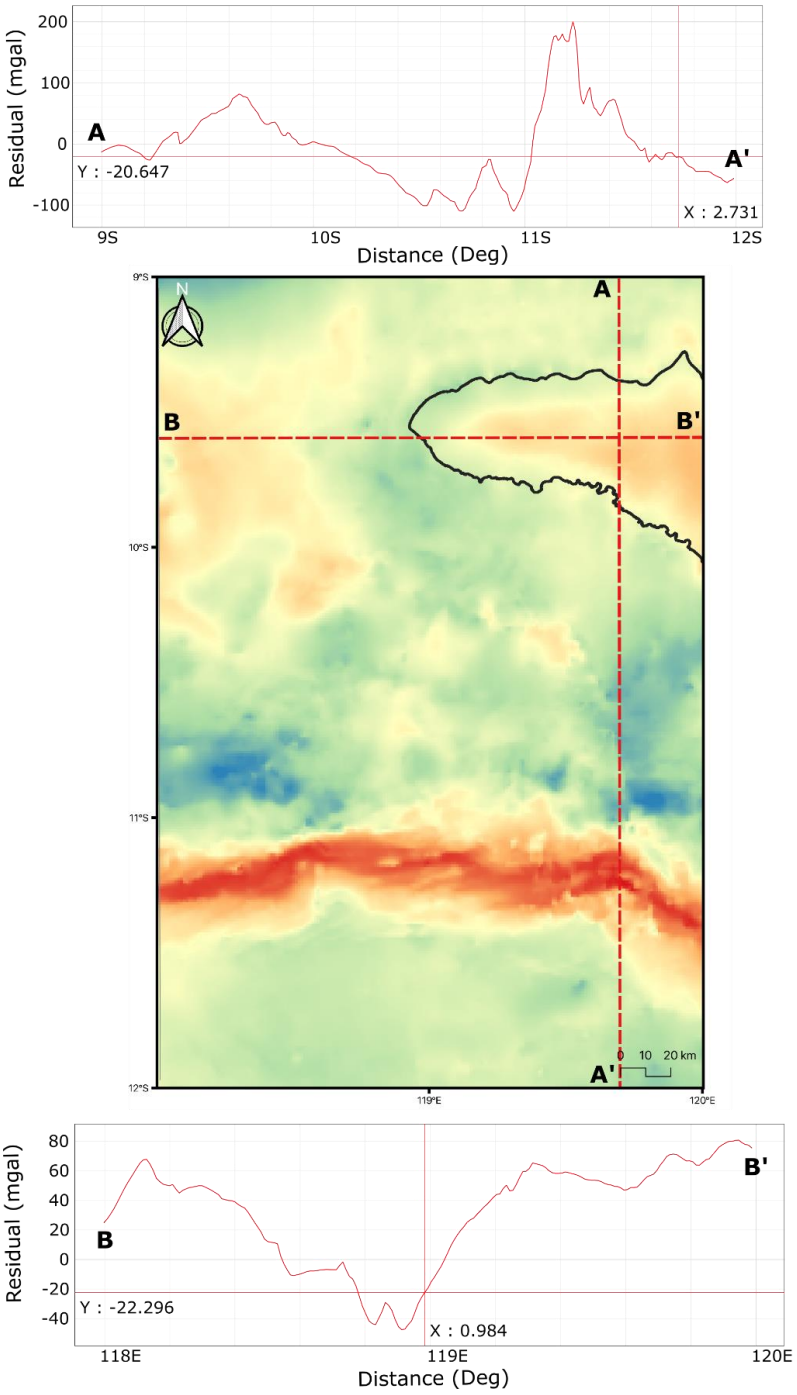

Figure 6. Cross-section profiles of residual anomalies along transects A-A' and B-B'. The X-axis represents the distance in degrees, while the Y-axis shows the residual anomaly values in mGal.

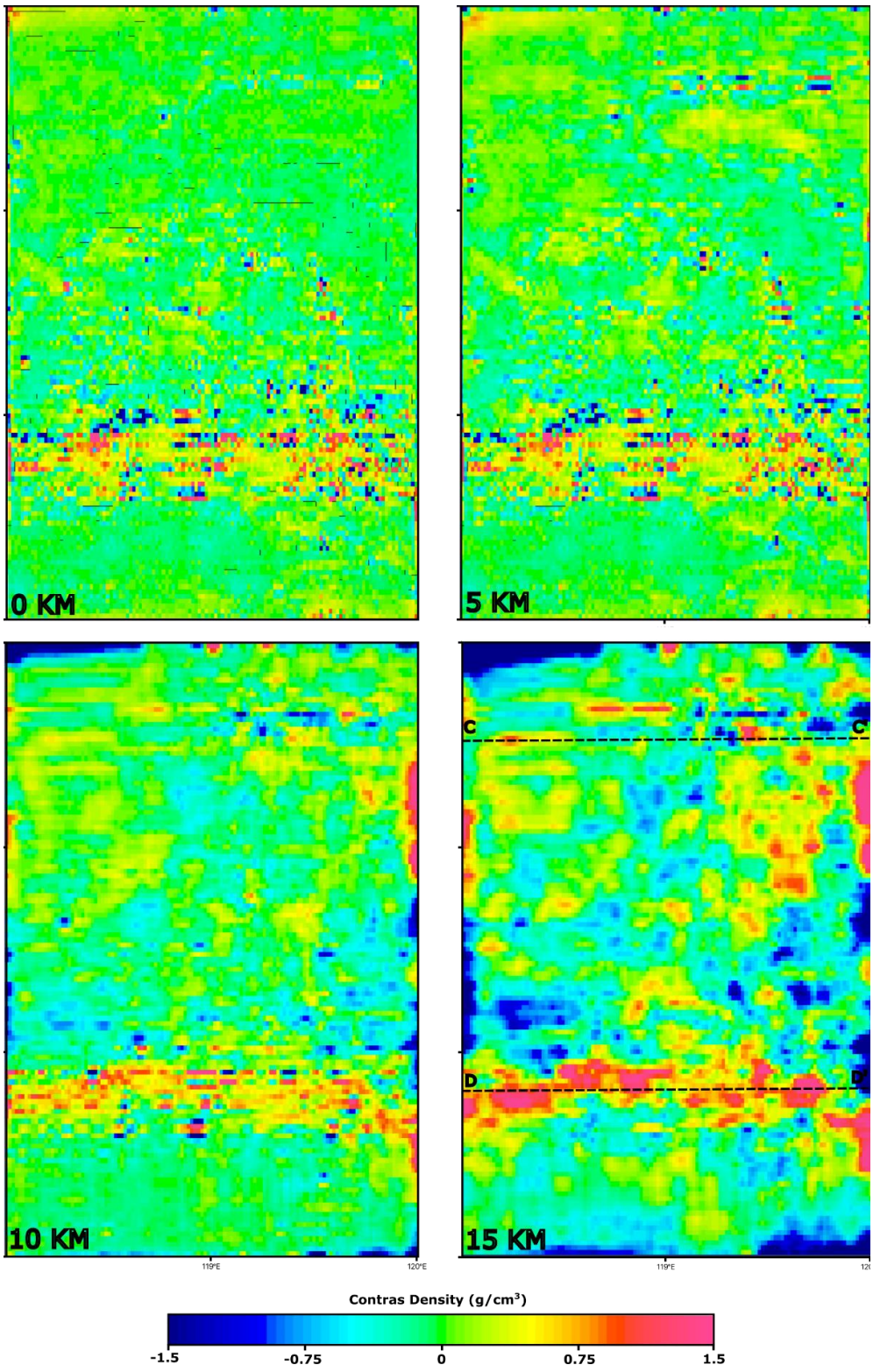

Figure 7. 3D density contrast modeling at depths of 0 km, 5 km, 10 km, and 15 km, represented in pixels with a view from the top. Dashed lines indicate profiles C-C' and D-D', as shown in Figure 8.

3D modelling based on gravity anomaly data was performed to understand the subsurface dimensionality better. The results of this modelling are represented as density contrasts at various depths, as shown in Figure 7. The density contrast ranges from -1.5 g/cm^3 to 1.5 g/cm^3. At the surface level (0 meters depth), the density contrast appears relatively homogeneous in the northern region, except for localized variations in the Java Trench area. As depth increases (5–10 km), the density contrast becomes more pronounced across the entire region. At a depth of 15 km, the density contrast in the subduction zone appears homogenized but with consistently high values, indicative of significant density variations in this tectonically active zone.

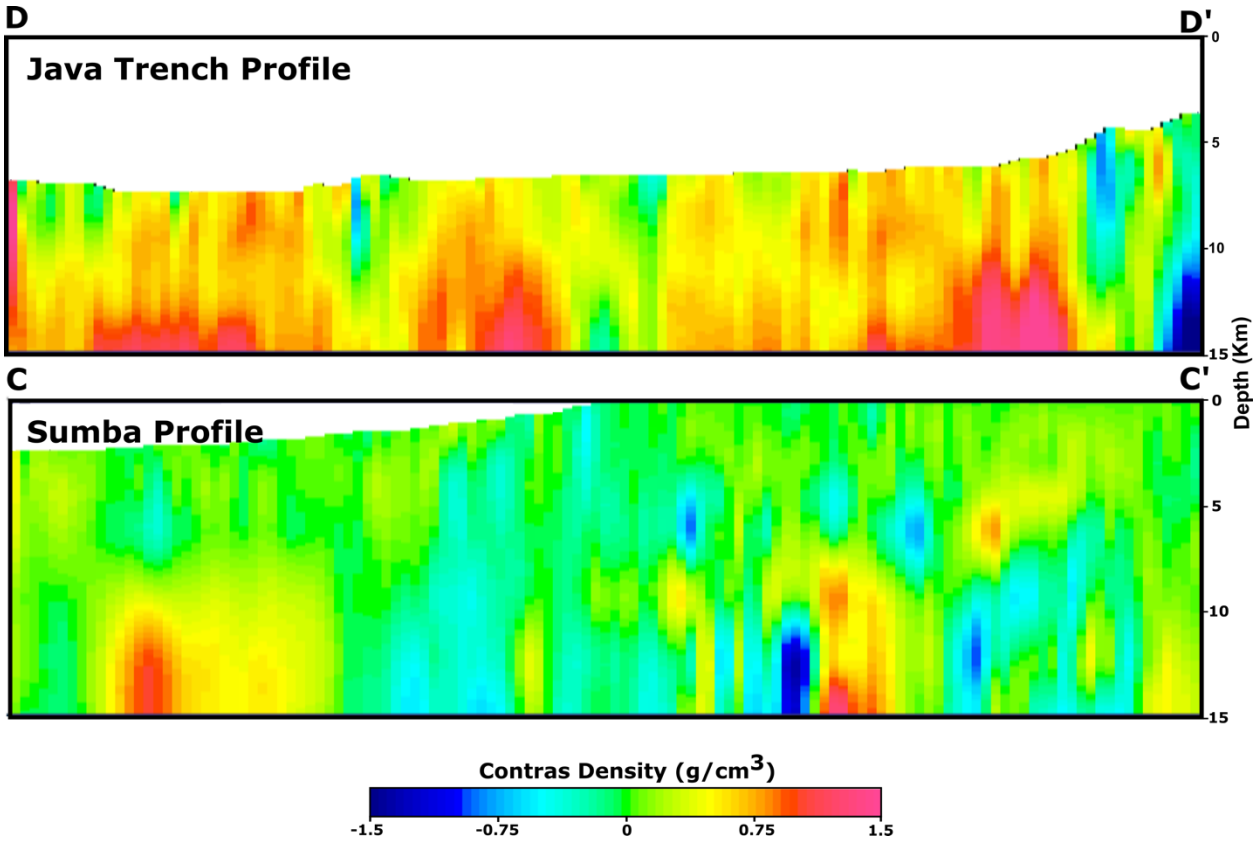

Figure 8. 2D line density contrast profiles derived from 3D modeling. The top profile corresponds to the Java Trench (subduction zone), while the bottom represents the Sumba Profile. Both profiles are vertically exaggerated for clarity.

Given the regions of interest—Sumba Island and the Java Trench—two 2D vertical profiles were extracted from the 3D modeling to provide detailed subsurface insights. These profiles, oriented west to east, are shown as C-C′ and D-D′ in Figure 8. The Sumba profile (C-C′), which focuses on the subsurface structure beneath Sumba Island, reveals that the first 5 km of depth is characterized by a homogeneous density contrast close to 0 g/cm^3. This suggests minimal density variation near the surface. However, at depths exceeding 5 km and extending to 15 km, the density contrast becomes more erratic, indicating significant heterogeneity in the deeper subsurface.

In contrast, the profile across the subduction zone (D-D') exhibits distinct characteristics. At depths shallower than 10 km, the density contrast remains moderate, but beyond 10 km, the density contrast increases significantly, reaching consistently high positive values of approximately 1.5 g/cm³. This high-density contrast likely reflects the presence of dense materials associated with subduction-related processes, such as the accumulation of mafic or ultramafic rocks. These 2D profiles provide valuable insights into the subsurface structures and the tectonic processes shaping the Sumba Island and Java Trench regions.

Based on the results of 3D modelling, it is insightful to compare the findings with the existing geological map, which represents the real geological conditions. Due to the lack of well data in the study area, the geological map of Sumba Island was used for this comparison, focusing on the western part of the island, as shown in Figure 9. Given that the background density for inland regions is approximately 2.67 g/cm³ and for oceanic regions is 1.04 g/cm³, the absolute density was estimated by adding the background density to the observed density contrast.

Profile C-C' spans from the ocean on the left to Sumba Island on the right, showing a density contrast ranging from -1.5 g/cm³ to 1.5 g/cm³. Over the oceanic region, most of the density contrast is positive (0–1.5 g/cm³), resulting in an absolute density range of 1.04–2.54 g/cm³, corresponding to water and igneous rocks. On the landward side of the profile, particularly below 5 km depth, the density contrast ranges between 0–0.375 g/cm³, producing an absolute density of 2.67–3.045 g/cm³. This range can be interpreted as a combination of sedimentary and igneous rocks, as shown in the density table of rocks and minerals [27]. The calculated density ranges were compared to the region's surface geology using the geological map to refine these interpretations.

The western Sumba region is dominated by three main geological formations: Reef Limestone (Pleistocene), Waikabubak Formation (Pliocene/Miocene), and Kananggar Formation (Pliocene/Miocene) [28]. The Reef Limestone, also known as the Kaliangga Formation, consists predominantly of reef sediments and is the primary formation on the outer parts of western Sumba. The Waikabubak Formation, located mainly in the central region of western Sumba, consists of extrusive igneous rocks, intermediate rocks, and pyroclastic materials. The Kananggar Formation, dominant in the southeastern part of Sumba, comprises clastic sedimentary rocks. The calculated absolute density range of 2.67–3.045 g/cm³ aligns well with these surface geological formations, validating the interpretations. Interestingly, along the same profile (C-C'), at depths exceeding 10 km, regions with very high-density contrast were observed, suggesting the presence of distinct subsurface structures that warrant further investigation.

The density contrast in the Java Trench region (Profile D-D') is predominantly 1.5 g/cm³. Considering the background density of water (1.04 g/cm³), the absolute density in this region is calculated as 2.54 g/cm³. This value corresponds to andesite, an igneous rock between felsic and mafic compositions. These results provide significant insights into the lithological and tectonic characteristics of the study area, contributing to a deeper understanding of its geological framework.

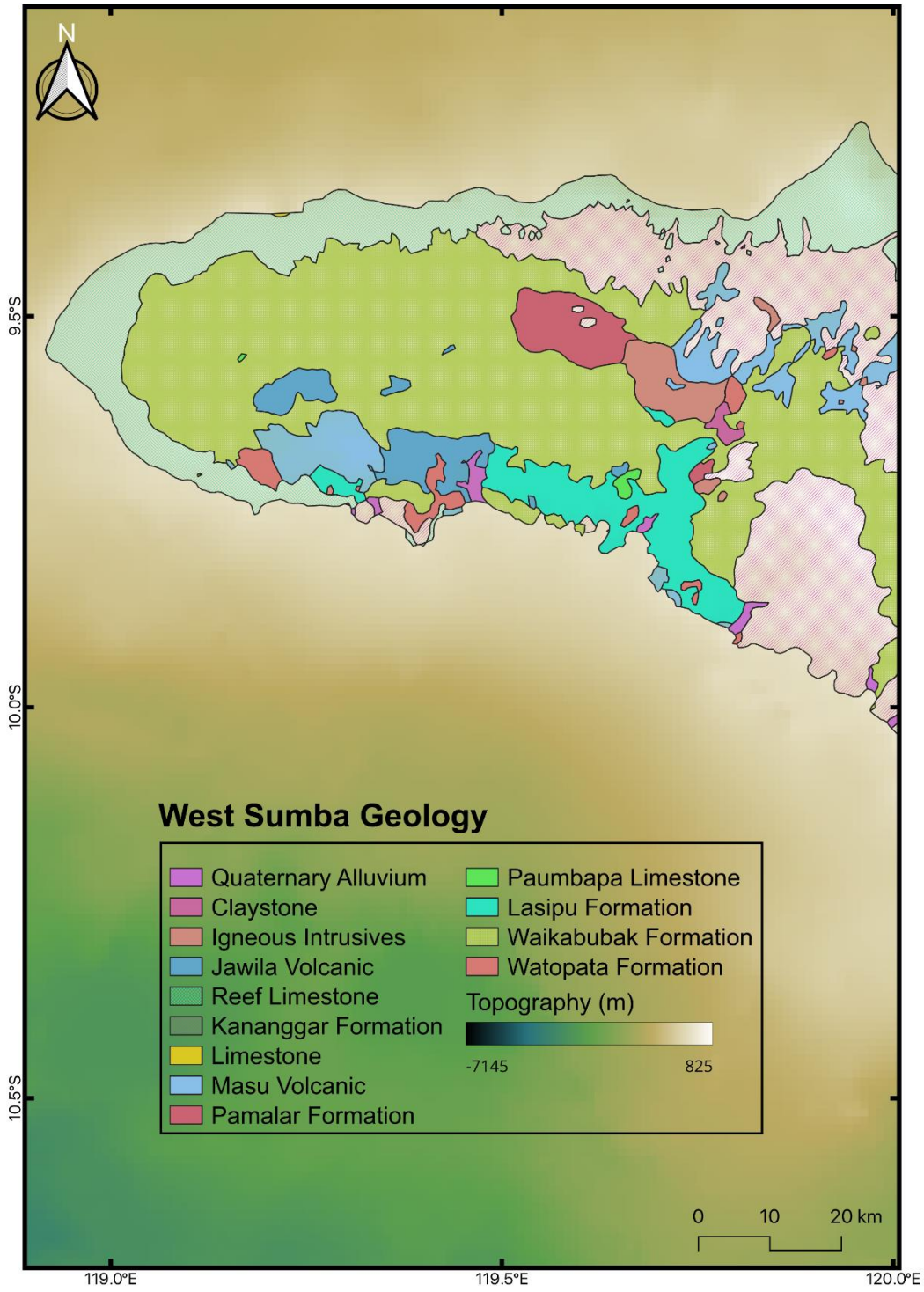

Figure 9. Geological map of the West Sumba region, adapted from [28], overlaid on a topographic map. The dominant formations in the West Sumba region—Reef Limestone, Kananggar Formation, and Waikabubak Formation—are represented with distinct fill styles. In contrast, other formations are shown with a solid fill style.

Conclusion

The residual anomaly was calculated using the Airy isostasy method, revealing that the Java Trench exhibits the highest residual anomaly values. The results of 3D gravity modeling in the western Sumba region align well with the dominant geological formations of the area, namely the Reef Limestone, Waikabubak Formation, and Kananggar Formation. Additionally, a region with a high-density contrast beneath Sumba Island indicates the potential for a distinct subsurface structure, which warrants further investigation to better understand its geological and tectonic significance.

Acknowledgment

The authors express their gratitude to the two anonymous reviewers for their invaluable suggestions and constructive feedback, which have significantly improved the quality of this paper. The figures presented in this study were created using QGIS Version 3.40.1 and Inkscape Version 1.3.2, which are free software tools, and Grav3D Version 2.0, a licensed software provided to Prof. Dr. Djoko Santoso (Bandung Institute of Technology) by the University of British Columbia (UBC).

References

[1] M. G. Audley-Charles, "Ocean trench blocked and obliterated by Banda forearc collision with Australian proximal continental slope," *Tectonophysics*, vol. 389, no. 1–2, pp. 65–79, Sep. 2004, doi: 10.1016/j.tecto.2004.07.048.

[2] R. Hall, "Australia–SE Asia collision: plate tectonics and crustal flow," *Geological Society of London*, vol. 355(1), no. Special Publications, pp. 75–109, 2011.

[3] P. Supendi *et al.*, "Fate of Forearc Lithosphere at Arc-Continent Collision Zones: Evidence from Local Earthquake Tomography of the Sunda-Banda Arc Transition, Indonesia," *Geophys Res Lett*, vol. 47, no. 6, Mar. 2020, doi: 10.1029/2019GL086472.

[4] W. J. F. Simons *et al.*, "A decade of GPS in Southeast Asia: Resolving Sundaland motion and boundaries," *J Geophys Res Solid Earth*, vol. 112, no. 6, Jun. 2007, doi: 10.1029/2005JB003868.

[5] H. Nugroho, R. Harris, A. W. Lestariya, and B. Maruf, "Plate boundary reorganization in the active Banda Arc-continent collision: Insights from new GPS measurements," *Tectonophysics*, vol. 479, no. 1–2, pp. 52–65, Dec. 2009, doi: 10.1016/j.tecto.2009.01.026.

[6] S. J. Hutchings and W. D. Mooney, "The Seismicity of Indonesia and Tectonic Implications," *Geochemistry, Geophysics, Geosystems*, vol. 22, no. 9, Sep. 2021, doi: 10.1029/2021GC009812.

[7] Hery. Harjono, *Seismotektonik busur Sunda*. LIPI Press, 2017.

[8] I. Sota, "Pendugaan Struktur Patahan Dengan Metode Gayaberat," *POSITRON*, vol. I, no. 1, pp. 25–30, 2011.

[9] Pusat Studi Gempa Nasional, *Peta Sumber dan Bahaya Gempa Indonesia Tahun 2017*. Pusat Penelitian dan Pengembangan Perumahan dan Pemukiman, Badan Penelitian dan Pengembangan, Kementerian Pekerjaan Umum dan Perumahan Rakyat, 2017.

[10] R. J. Blakely, *Potential Theory in Gravity and Magnetic Applications*. Cambridge University Press, 1995.

[11] Lee-Lueng Fu, "TOPEX/POSEIDON mission overview," *J Geophys Res*, vol. 99, no. C12, 1994, doi: 10.1029/94jc01761.

[12] P. N. A. M. Visser, "Gravity Field Determination with Goce And Grace," 1999. [Online]. Available: www.elsevier.nMocate/asr

[13] C. Hirt, M. Kuhn, S. Claessens, R. Pail, K. Seitz, and T. Gruber, "Study of the Earth's short-scale gravity field using the ERTM2160 gravity model," *Comput Geosci*, vol. 73, pp. 71–80, 2014, doi: 10.1016/j.cageo.2014.09.001.

[14] M. Gilardoni, M. Reguzzoni, and D. Sampietro, "GECO: a global gravity model by locally combining GOCE data and EGM2008," *Studia Geophysica et Geodaetica*, vol. 60, no. 2, pp. 228–247, Apr. 2016, doi: 10.1007/s11200-015-1114-4.

[15] R. Margiono, A. Novitri, A. Pevriadi, and H. Zakariya, "Analisis Data Gravitasi Untuk Identifikasi Sesar Lokal Penyebab Gempabumi Di Wilayah Barat Daya Sumba Indonesia," *Jurnal Meteorologi dan Geofisika*, vol. 22, no. 2, pp. 67–73, 2021, [Online]. Available: http://puslitbang.bmkg.go.id/jmg/index.php/jmg/article/view/824

[16] A. K. Maimuna, E. A. Pramesthi, Y. A. Segoro, and ..., "Analisis Anomali Gaya Berat Menggunakan Metode SVD dan Pemodelan 3D (Studi Kasus Gempa di Kepulauan Togean, Kabupaten Tojo Una-Una, Sulawesi …," *Jurnal Geofisika*, vol. 19, no. 01, pp. 17–23, 2021, [Online]. Available: https://178.128.59.82/index.php/jurnal-geofisika/article/view/466

[17] H. Zakariya, R. Margiono, A. Novitri, and A. Pevriadi, "Identifikasi Anomali Gravitasi Di Wilayah Sulawesi Tenggara Berdasarkan Data Gravitasi GGMplus," *PROGRESS: Jurnal Geofisika*, vol. 1, no. 1 SE-Articles, pp. 63–68, Jun. 2022, [Online]. Available: https://stmkg.balai2bmkg.id/index.php/pjg/article/view/24

[18] S. Maus and V. Dimri, "Depth estimation from the scaling power spectrum of potential fields?" *Geophys J Int*, vol. 124, no. 1, pp. 113–120, 1996, doi: 10.1111/j.1365-246X.1996.tb06356.x.

[19] B. G. Dewanto, R. Margiono, Y. A. Segoro, E. Pramesthi, and A. K. Maimuna, "The importance of gravity data for estimating and identifying the sediment thickness of subsurface structure around Majene Sulawesi Barat," in *AIP Conference Proceedings*, American Institute of Physics Inc., Feb. 2023. doi: 10.1063/5.0115361.

[20] D. T. Sandwell and W. H. F. Smith, "Global marine gravity from retracked Geosat and ERS-1 altimetry: Ridge segmentation versus spreading rate," *J Geophys Res Solid Earth*, vol. 114, no. 1, Jan. 2009, doi: 10.1029/2008JB006008.

[21] E. S. Garcia, D. T. Sandwell, and W. H. F. Smith, "Retracing cryostat-2, Envisat and Jason-1 radar altimetry waveforms for improved gravity field recovery," *Geophys J Int*, vol. 196, no. 3, pp. 1402–1422, Mar. 2014, doi: 10.1093/gji/ggt469.

[22] D. T. Sandwell, R. D. Müller, W. H. F. Smith, E. Garcia, and R. Francis, "New global marine gravity model from CryoSat-2 and Jason-1 reveals buried tectonic structure," *Science (1979)*, vol. 346, no. 6205, pp. 65–67, Oct. 2014, doi: 10.1126/science.1258213.

[23] D. S. Parasnis, *Principles of Applied Geophysics*, Fourth. Springer Dordrecht, 1986. Doi: https://doi.org/10.1007/978-94-009-4113-7.

[24] S. R. Soler and L. Uieda, "Gradient-boosted equivalent sources," *Geophys J Int*, vol. 227, no. 3, pp. 1768–1783, Dec. 2021, doi: 10.1093/gji/ggab297.

[25] F. a Terra Project *et al.*, "Harmonica v0.7.0: Forward modeling, inversion, and processing gravity and magnetic data," Aug. 2024, *Zenodo*. doi: 10.5281/zenodo.13308312.

[26] Y. Li and D. W. Oldenburg, "3-D inversion of gravity data," 1998. [Online]. Available: http://segdl.org/

[27] P. V Sharma, *Environmental and Engineering Geophysics*. Cambridge: Cambridge University Press, 1997. doi: DOI: 10.1017/CBO9781139171168.

[28] E. Rutherford, K. Burke, and J. Lytwyn, "Tectonic history of Sumba Island, Indonesia, since the Late Cretaceous and its rapid escape into the forearc in the Miocene." [Online]. Available: www.elsevier.nl/locate/jseaes